

A NEW MILKY WAY SATELLITE DISCOVERED IN THE SUBARU/HYPER SUPRIME-CAM SURVEY

DAISUKE HOMMA¹, MASASHI CHIBA¹, SAKURAKO OKAMOTO², YUTAKA KOMIYAMA^{3,4}, MASAYUKI TANAKA³, MIKITO TANAKA¹, MIHO N. ISHIGAKI⁵, MASAYUKI AKIYAMA¹, NOBUO ARIMOTO^{6,4}, JOSÉ A. GARMILLA⁷, ROBERT H. LUPTON⁷, MICHAEL A. STRAUSS⁷, HISANORI FURUSAWA³, SATOSHI MIYAZAKI^{3,4}, HITOSHI MURAYAMA⁵, ATSUSHI J. NISHIZAWA⁸, MASAHIRO TAKADA⁵, TOMONORI USUDA^{3,4}, AND SHIANG-YU WANG⁹

Draft version October 4, 2018

ABSTRACT

We report the discovery of a new ultra-faint dwarf satellite companion of the Milky Way based on the early survey data from the Hyper Suprime-Cam Subaru Strategic Program. This new satellite, Virgo I, which is located in the constellation of Virgo, has been identified as a statistically significant (5.5σ) spatial overdensity of star-like objects with a well-defined main sequence and red giant branch in their color-magnitude diagram. The significance of this overdensity increases to 10.8σ when the relevant isochrone filter is adopted for the search. Based on the distribution of the stars around the likely main sequence turn-off at $r \sim 24$ mag, the distance to Virgo I is estimated as 87 kpc, and its most likely absolute magnitude calculated from a Monte Carlo analysis is $M_V = -0.8 \pm 0.9$ mag. This stellar system has an extended spatial distribution with a half-light radius of 38_{-11}^{+12} pc, which clearly distinguishes it from a globular cluster with comparable luminosity. Thus, Virgo I is one of the faintest dwarf satellites known and is located beyond the reach of the Sloan Digital Sky Survey. This demonstrates the power of this survey program to identify very faint dwarf satellites. This discovery of Virgo I is based only on about 100 square degrees of data, thus a large number of faint dwarf satellites are likely to exist in the outer halo of the Milky Way.

Subject headings: galaxies: dwarf — galaxies: individual (Virgo) — Local Group

1. INTRODUCTION

Dwarf spheroidal galaxies (dSphs) associated with the Milky Way (MW) and Andromeda galaxies provide important constraints on the role of dark matter in galaxy formation and evolution. Indeed, these faint stellar systems are largely dominated by dark matter with mass-to-luminosity ratios of 10 to 1000 or even larger in fainter systems, based on their stellar dynamics (Gilmore et al. 2007; Simon & Geha 2007). Thus, the basic properties of dSphs, such as their total number and spatial distributions inside a host halo like the MW, provide useful constraints on dark matter on small scales, in particular the nature and evolution of cold dark matter (CDM) in a Λ dominated universe.

One of the tensions between theory and observation is the missing satellite problem: the theory predicts a much larger number of subhalos in a MW-like halo than

the observed number of satellite galaxies (Klypin et al. 1999; Moore et al. 1999). Solutions to this problem are to consider other types of dark matter than CDM (e.g., Macciò & Fontanot 2010) or to invoke baryonic physics (e.g., Sawala et al. 2016). Another possibility is that we have seen only a fraction of all the satellites associated with the MW due to various observational biases (Tollerud et al. 2008). Motivated by this, a systematic search for new dSphs has been made based on large survey programs, such as the Sloan Digital Sky Survey (SDSS) (York et al. 2000) and the Dark Energy Survey (DES) (Abbott et al. 2016). SDSS discovered 15 ultra-faint dwarf galaxies (UFDs) with $M_V \gtrsim -8$ mag (e.g., Willman et al. 2005; Sakamoto & Hasegawa 2006; Belokurov et al. 2006), and DES recently reported the discovery of many more candidate UFDs in the south (e.g., Bechtol et al. 2015; Koposov et al. 2015; Drlica-Wagner et al. 2015). These discoveries are consistent with the work by Tollerud et al. (2008), anticipating that there exists a large number of yet unidentified dwarf satellites in the MW halo, especially in its outer parts.

This paper reports the discovery of a new faint dwarf satellite in the MW, in the course of the Subaru Strategic Program (SSP) using Hyper Suprime-Cam (HSC). HSC is a new prime-focus camera on the Subaru telescope with a 1.5 deg diameter field of view (Miyazaki et al. 2012), which thus allows us to survey a large volume of the MW halo out to a large distance from the Sun, where a systematic search for new satellites has not yet been undertaken.

2. DATA AND METHOD

The HSC-SSP is an ongoing optical imaging survey, which consists of three layers with different combinations of area and depth. Our search for new MW satellites is

¹ Astronomical Institute, Tohoku University, Aoba-ku, Sendai 980-8578, Japan

E-mail: d.homma@astr.tohoku.ac.jp

² Shanghai Astronomical Observatory, 80 Nandan Road, Shanghai 200030, China

³ National Astronomical Observatory of Japan, 2-21-1 Osawa, Mitaka, Tokyo 181-8588, Japan

⁴ The Graduate University for Advanced Studies, Osawa 2-21-1, Mitaka, Tokyo 181-8588, Japan

⁵ Kavli Institute for the Physics and Mathematics of the Universe (WPI), The University of Tokyo, Kashiwa, Chiba 277-8583, Japan

⁶ Subaru Telescope, National Astronomical Observatory of Japan, 650 North A'ohoku Place, Hilo, HI 96720, USA

⁷ Princeton University Observatory, Peyton Hall, Princeton, NJ 08544, USA

⁸ Institute for Advanced Research, Nagoya University, Furocho, Chikusa-ku, Nagoya 464-8602, Japan

⁹ Institute of Astronomy and Astrophysics, Academia Sinica, Taipei, 10617, Taiwan

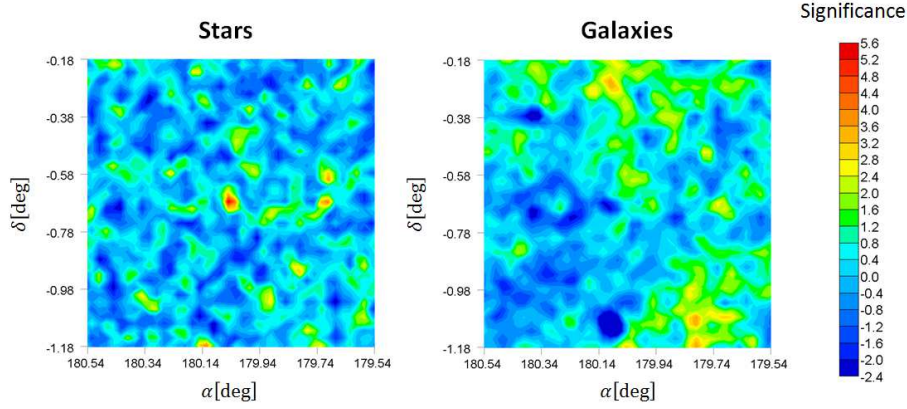


FIG. 1.— Left panel: the spatial distribution of the sources classified as stars with $i < 24.5$ mag and $g - r < 1.0$, covering one square degree centered on the candidate overdensity of stars. The star counts are in bins of $0''.05 \times 0''.05$. Right panel: the plot for the sources classified as galaxies with $i < 24.5$ mag and $g - r < 1.0$. Note that there is no overdensity at the center of this plot.

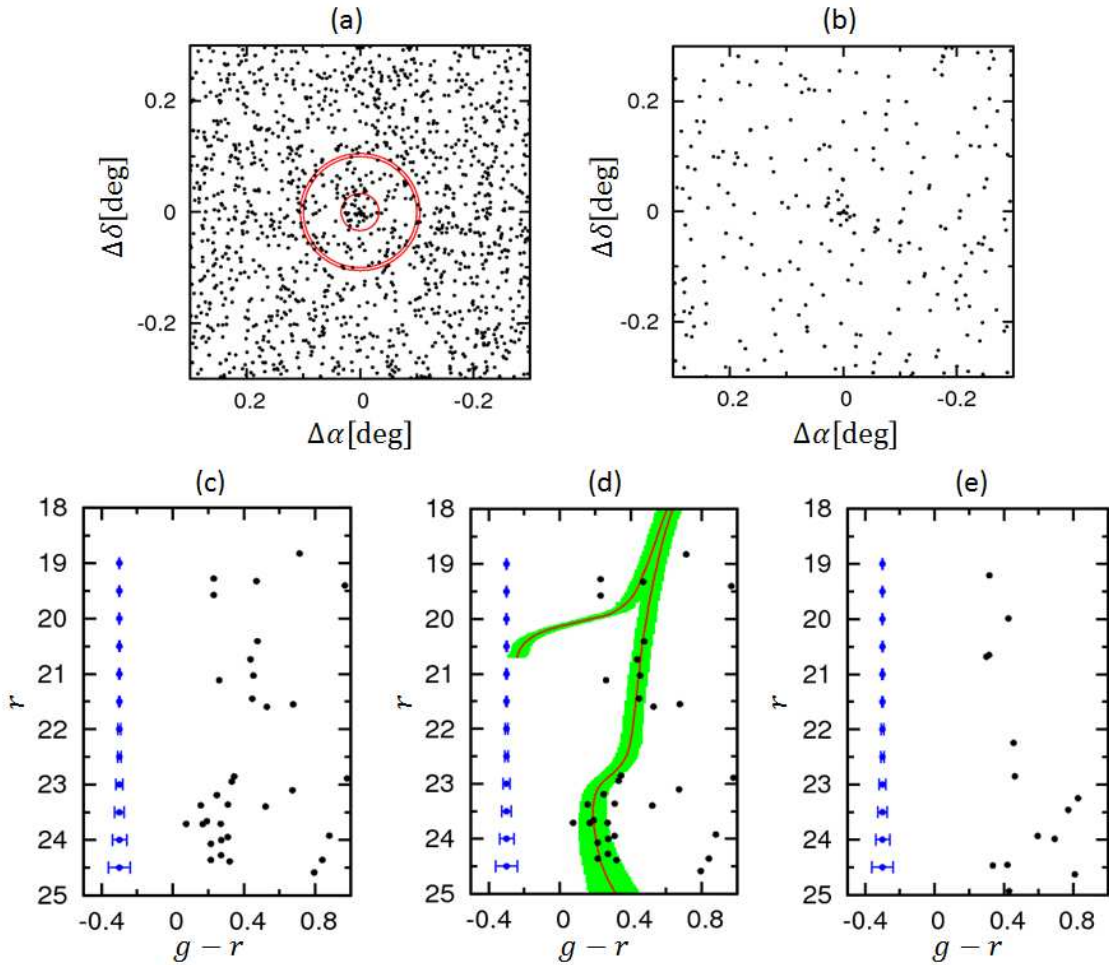


FIG. 2.— The spatial distribution of the stars around the overdensity (upper panels, where $\Delta\alpha$ and $\Delta\delta$ are the relative offsets in celestial coordinates) and their distribution in the $g - r$ vs. r CMD (lower panels). Panel (a): spatial distribution of the sources classified as stars with $i < 24.5$ mag and $g - r < 1.0$. Red circles denote annuli with radii $= 2'$, $6'$, and $6''.33$ from the center. There is an overdensity around the field center with statistical significance of 5.5 . Panel (b): the same as (a) but for the stars passing the isochrone filter shown in panel (d). The statistical significance of the overdensity, 10.8 , is higher than in panel (a). Panel (c): CMD for the stars at $r < 2'$, where the error bars show a typical measurement error in color at each r magnitude. Panel (d): the same as (c) but including an isochrone (red line) for an old, metal-poor system [age of 13 Gyr and metallicity of $[M/H] = -2.2$ at a distance modulus of $(m - M)_0 = 19.7$ mag]. The shaded area covers both the typical photometric error and likely intrinsic dispersion of the CMD in star clusters. Panel (e): the same as (c) but for field stars at $6' < r < 6''.33$, which has the same solid angle. Note the absence of a main sequence turn-off.

based on its Wide layer, aiming to observe $\sim 1400 \text{ deg}^2$ in five photometric bands (g , r , i , z , and y), where the

target 5σ point-source limiting magnitudes are (g , r , i , z , y) = (26.5, 26.1, 25.9, 25.1, 24.4) mag. In this paper, we

utilize the (g, r) data in the early HSC survey obtained before 2015 November, covering $\sim 100 \text{ deg}^2$ in 5 fields along the celestial equator. The HSC data are processed with `hscPipe v4.0.1`, a branch of the Large Synoptic Survey Telescope pipeline (Ivezic et al. 2008; Juric et al. 2015) calibrated against PanSTARRS1 photometry and astrometry (Schlafly et al. 2012; Tonry et al. 2012; Magnier et al. 2013).

We use the *extendedness* parameter from the pipeline to select point sources. This parameter is computed from the ratio between PSF and `cmodel` fluxes, which are measured by fitting PSF models and two-component PSF-convolved galaxy models to the source profile, respectively (Abazajian et al. 2004). When the ratio between these fluxes is larger than 0.985, a source is classified as a point source. We use the parameter measured in the i -band, in which the seeing is typically the best of our five filters with a median of about $0''.6$. In particular, the i -band seeing for the region around our new-found satellite is about $0''.5$. In order to characterize the completeness and contamination of our star/galaxy classification, we stack the COSMOS data (COSMOS is one of our UltraDeep fields, where we have many exposures) to the depth of the Wide survey and compare our classification against the HST/ACS data from Leauthaud et al. (2007). We find that the completeness, defined here as the fraction of objects that are classified as stars by ACS, and correctly classified as stars by HSC, is above 90% at $i < 22.5$, and drops to $\sim 50\%$ at $i = 24.5$. On the other hand, contamination, which is defined as the fraction of HSC-classified stars which are classified as galaxies by ACS, is close to zero at $i < 23$, but increases to $\sim 50\%$ at $i = 24.5$. Based on this test, we choose to use the extendedness parameter down to $i = 24.5$ to select stars in this work¹⁰. We further apply a $g - r < 1.0$ cut to eliminate numerous M-type disk stars.

In order to search for the signature of new satellites, we count stars in $0''.05 \times 0''.05$ bins in right ascension and declination, with an overlap of $0''.025$ in each direction, where $0''.05$ corresponds to a typical half-light diameter ($\sim 80 \text{ pc}$) of an ultra-faint dwarf at a distance of 90 kpc. We then calculate the mean density and its dispersion over all cells for each of the Wide layer fields to search for any spatial overdensities of stars (e.g., Koposov et al. 2008; Walsh et al. 2009). The deviation from the mean density has close to a Gaussian distribution. We have found one stellar overdensity with 5.5σ in one of the Wide layer fields. The standard deviation is estimated separately for each survey field (covering typically 20 to 30 deg^2); each field is at different Galactic coordinates. This overdensity is centered at $(\alpha, \delta) = (180^\circ.04, -0^\circ.68)$. As Figure 1 shows, there is no corresponding overdensity in extended objects (galaxies)¹¹.

¹⁰ Another method for star/galaxy classification by combining the colors of the sources (Garmilla et al. in prep.) has also been applied and we have confirmed that the main results of this work remain unchanged. The full description for the analysis of the data based on this alternative scheme will be presented in a future paper.

¹¹ Another high-sigma overdensity (6.8σ) of the sources with **extendedness** = 0 has been identified in the survey region, but this appears an artefact related to scattered light from a nearby bright star.

In Figure 2(a), we plot the spatial distribution of the stars around this overdensity, which shows a localized concentration of stars within a circle of radius $2'$. To get further insights into this overdensity, in Figure 2(c), we plot the $(g - r, r)$ color-magnitude diagram (CMD) of stars within the $2'$ radius circle shown in Figure 2(a). This CMD shows signatures of main sequence (MS) stars near its turn off (MSTO) as well as stars on the red giant branch (RGB), whereas these features disappear when we plot stars at $6' < r < 6'.33$ with the same solid angle, i.e. likely field stars outside the overdensity, as shown in Figure 2(e). To investigate the distribution of the overdensity in the CMD further, we adopt a fiducial locus of stars in a typical ultra-faint dwarf galaxy based on a PARSEC isochrone (Bressan et al. 2012), in which we assume an age of 13 Gyr and metallicity of $z = 0.0001$ ($[M/H] = -2.2$). We first derive this isochrone in the SDSS filter system and then convert to the HSC filter system using the following formula calibrated from both filter curves and spectral atlas of stars (Gunn & Stryker 1983), $g = g_{\text{SDSS}} - a(g_{\text{SDSS}} - r_{\text{SDSS}}) - b$ and $r = r_{\text{SDSS}} - c(r_{\text{SDSS}} - i_{\text{SDSS}}) - d$, where $(a, b, c, d) = (0.074, 0.011, 0.004, 0.001)$ and the subscript SDSS denotes the SDSS system. This isochrone, at the assumed distance modulus of $(m - M)_0 = 19.7 \text{ mag}$ as determined below, is shown in Figure 2(d), which does a good job of tracing the distributions of MSTO and RGB stars. To test the statistical significance of the overdensity along this isochrone, we set the selection filter defined by the CMD envelope [shaded region in Figure 2(d)], which consists of the above isochrone, 1σ $(g - r)$ color measurement error as a function of r -band magnitude, and a typical color dispersion of about $\pm 0.05 \text{ mag}$ at the location of the RGB arising from a metallicity dispersion of $\pm 0.7 \text{ dex}$ for dSph stars. By passing this filter over the stars in the relevant region, we derive an overdensity that peaks at a distance modulus of 19.7 mag at a statistical significance of 10.8σ , much higher than without the filter. Figure 2(b) shows the distribution of the stars that pass this filter, revealing a higher overdensity contrast than Figure 2(a). This suggests that the overdensity we have found here is indeed an old stellar system, either a globular cluster or dwarf galaxy. Hereafter we refer to this system as Virgo I¹². The stars selected by this isochrone filter lie along a clear stellar sequence even in a 2-color $(g - r, r - i)$ diagram. We note that the statistical significance of this overdensity before (after) passing this isochrone filter remains basically unchanged when we adopt different magnitude limits for the sample: 5.6σ (10.3σ) for $i < 24 \text{ mag}$ and 4.8σ (9.6σ) for $i < 25 \text{ mag}$.

3. PROPERTIES OF STELLAR POPULATION

We estimate the basic structural properties of Virgo I. For this purpose, we adopt six parameters $(\alpha_0, \delta_0, \theta, \epsilon, r_h, N_*)$: (α_0, δ_0) for the celestial coordinates of the centroid of the overdensity, θ for its position angle from north to east, ϵ for the ellipticity, r_h for the half-light radius, and N_* for the number of stars belonging to the overdensity. The maximum likelihood method of Martin et al. (2008) is applied to the stars within a circle

¹² This is not to be confused with the so-called Virgo overdensity, which is closer at ~ 6 to 20 kpc and covering a much larger volume (Juric et al. 2008).

TABLE 1
PROPERTIES OF VIRGO I

| Parameter ^a | Value |
|--|---|
| Coordinates (J2000) | 12 ^h 00 ^m 09 ^s .6, -0°40′48″ |
| Galactic Coordinates (l , b) | 276°.94, 59°.58 |
| Position angle | +51 ⁺¹⁸ ₋₄₀ deg |
| Ellipticity | 0.44 ^{+0.14} _{-0.17} |
| A_V | 0.066 mag |
| (m - M) ₀ | 19.7 ^{+0.3} _{-0.2} mag |
| Heliocentric distance | 87 ⁺¹³ ₋₈ kpc |
| Half light radius, r_h | 1′.5 ± 0′.4 or 38 ⁺¹² ₋₁₁ pc |
| M _{tot,V} | -0.8 ± 0.9 mag |

^a Integrated magnitudes are corrected for the mean Galactic foreground extinction, **A_V** (Schlafly & Finkbeiner 2011).

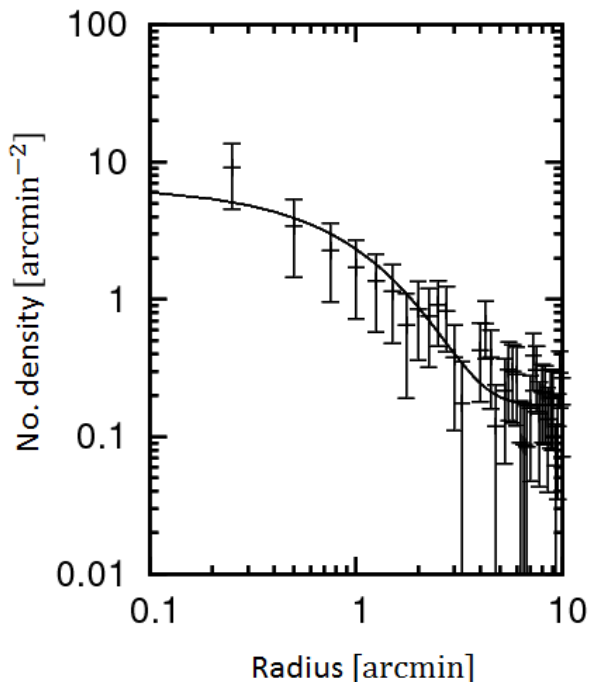


FIG. 3.— Density profile of the stars in Virgo I that pass the isochrone filter shown in Figure 2(b), in elliptical annuli as a function of mean radius, where the uncertainties are derived assuming Poisson statistics. The line shows a fitted exponential profile with $r_h = 1'.5$.

of radius 20' passing the isochrone filter; the results are summarized in Table 1.

Figure 3 shows the radial profile of the stars passing the isochrone filter [Figure 2(b)] by computing the average density within elliptical annuli. The overplotted line corresponds to the best-fit exponential profile with a half-light radius of $r_h = 1'.5$ or 38 pc. This spatial size is larger than the typical size of MW globular clusters but is consistent with the scale of dwarf satellites as examined below.

The total absolute magnitude of Virgo I, M_V , is estimated by summing the luminosities of the stars within the half-light radius, r_h , and then doubling the summed luminosity (e.g., Sakamoto & Hasegawa 2006). For the transformation from (g, r) to V , we adopt the formula in Jordi et al. (2006) calibrated for metal-poor Population II, which are appropriate for stars in ultra-faint dwarf

galaxies. Assuming that the distance to this stellar system is 87 kpc or $(m - M)_0 = 19.7$ mag, we obtain $M_V = -0.17$ mag for $r_h = 1'.5$. This value varies when we adopt different half-light radii or different distance moduli within their 1σ uncertainties. We find $M_V = +0.08$ mag if we adopt $r_h = 1'.1$ and $(m - M)_0 = 19.5$ mag and $M_V = -1.87$ mag for $r_h = 1'.9$ and $(m - M)_0 = 20.0$ mag. The latter case yields a much brighter M_V due to the inclusion of a bright RGB star inside the aperture.

Shot noise due to the small number of stars in Virgo I is a significant additional source of uncertainty in M_V . We quantify this and other sources of error using a Monte Carlo method similar to that described in Martin et al. (2008) to determine the most likely value of M_V and its uncertainty. As summarized in Table 1 for Virgo I, we have derived $N_* = 19 \pm 5$ at $i < 24.5$ mag, the distance modulus of $(m - M)_0 = 19.7^{+0.3}_{-0.2}$ mag, and we use a stellar population model with an age of 13 Gyr and metallicity of $[M/H] = -2.2$. Based on these information, we generate 10^4 realizations of CMDs for three different initial mass functions (IMFs); Salpeter, Kroupa, and Chabrier (lognormal) (Salpeter 1995; Kroupa 2002; Chabrier 2001). We then derive the luminosity of the stars for each CMD at $i < 24.5$ mag, taking into account the completeness of the observed stars with HSC. Based on this Monte Carlo simulation, we obtain the expected values of M_V as $M_V = -0.82 \pm 0.95$, $M_V = -0.81 \pm 0.91$, and $M_V = -0.83 \pm 0.92$, for Salpeter, Kroupa, and Chabrier IMFs, respectively. Thus, the values of M_V for these different IMF models are consistent each other, summarized as $M_V = -0.8 \pm 0.9$ mag, and are within the 1σ uncertainty of M_V determined above by directly counting the observed member stars.

We note that the above models suggest the ratio between the number of RGB+HB and that of MSTO stars is about 0.2, whereas the observed ratio is about 0.4. This discrepancy by a factor of 2 can be understood when we consider the contamination of some field RGBs and/or incompleteness of faint MSTO stars.

4. DISCUSSION

To assess if Virgo I identified here is indeed a new MW dwarf satellite galaxy, we compare its size quantified by r_h with globular clusters with comparable luminosity, in the range of $M_V \sim +0.10$ to -1.72 mag. In Figure 4(a), we plot the relation between M_V and r_h for the MW globular clusters (dots) taken from Harris (1996), and dwarf galaxies in the MW (filled squares) and M31 (open squares) from McConnachie (2012), the recent DES work (Bechtol et al. 2015; Koposov et al. 2015; Drlica-Wagner et al. 2015), and other recent discoveries (Laevens et al. 2014; Kim et al. 2015; Kim & Jerjen 2015; Laevens et al. 2015a,b). The red star with error bars shows Virgo I detected in this work.

As is clear from the figure, the current stellar system is systematically larger than MW globular clusters with comparable M_V and is located along the locus of the MW and M31 dwarf galaxies. This is the case even if we adopt the brighter estimate of $M_V = -1.72$ mag by considering the 1σ uncertainty in M_V . Thus, the overdensity of the stars we have found here is a candidate ultra-faint dwarf galaxy. This is also supported from its non-zero ellipticity of $\epsilon = 0.44^{+0.14}_{-0.17}$, which is more similar to those of dwarf galaxies than globular clusters.

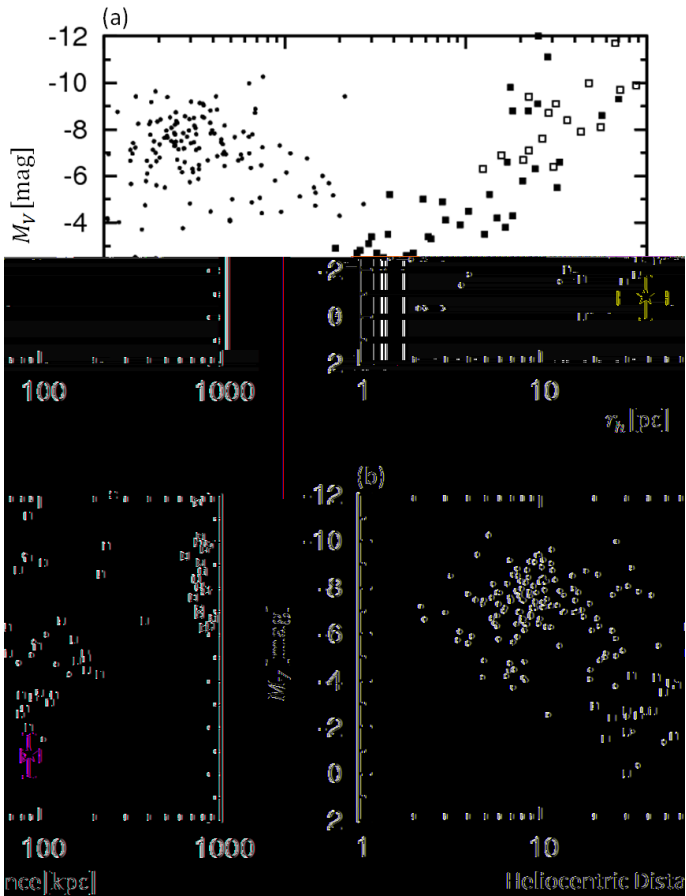


FIG. 4.— (a) The relation between M_V and r_h for stellar systems. Dots denote globular clusters in the MW taken from Harris (1996). Filled and open squares denote the MW and M31 dSphs, respectively, taken from McConnachie (2012), the recent DES work for new ultra-faint MW dSphs (Bechtol et al. 2015; Koposov et al. 2015; Drlica-Wagner et al. 2015), and other recent discoveries (Laevens et al. 2014; Kim et al. 2015; Kim & Jerjen 2015; Laevens et al. 2015a,b). The red star with error bars corresponds to the overdensity described in this paper, Virgo I, which lies within the locus defined by dSphs. (b) The relation between M_V and heliocentric distance for the systems shown in panel (a).

The heliocentric distance to Virgo I is $D = 87_{-8}^{+13}$ kpc, where the error estimate is derived from the range of the distance yielding the 1σ decrease in the statistical significance of Virgo I after passing the isochrone filter [defined in Figure 2(d)] from its peak value of 10.8σ . This distance is beyond the reach of previous surveys for MW dwarfs with comparable luminosity. This is demonstrated in Figure 4, which shows the relation between M_V and D for the MW and M31 dwarfs as well as the MW globular clusters.

5. CONCLUSIONS

We have identified a new ultra-faint dwarf satellite of the MW, Virgo I, in the constellation of Virgo. The satellite is located at a heliocentric distance of 87 kpc and its absolute magnitude in the V band is estimated as $M_V = -0.8 \pm 0.9$ mag, which is comparable to or fainter than that of the faintest dwarf satellite, Segue 1. The half-light radius of Virgo I is estimated to be ~ 38 pc, significantly larger than globular clusters with the

same luminosity, suggesting that it is a dwarf galaxy. To set further constraints on Virgo I, follow-up spectroscopic studies of bright RGB stars will be useful to investigate their membership and to determine the chemical and dynamical properties in this dwarf satellite.

Virgo I is located beyond the reach of the SDSS: its limiting magnitude of $r = 22.2$ implies that the completeness radius beyond which a faint dwarf galaxy like Virgo I will not be detected (Tollerud et al. 2008) is 28 kpc. With Subaru/HSC, this completeness radius for Virgo I is estimated as 89 kpc, if we adopt the limiting i -band magnitude of 24.5 mag combined with a typical $(r - i)$ color of $\simeq 0.2$. Thus, Virgo I with $D = 87_{-8}^{+13}$ kpc is located just at the edge where Subaru/HSC can reach. We therefore expect the presence of yet unidentified faint satellites in the outer parts of the MW halo as the HSC survey continues. Deep imaging surveys for these faint and distant satellites are indeed important to get further insights into their true number and thus the nature of dark matter on small scales.

We thank the referee for his/her helpful comments and suggestions. This work is supported in part by JSPS Grant-in-Aid for Scientific Research (B) (No. 25287062) and MEXT Grant-in-Aid for Scientific Research on Innovative Areas (No. 15H05889).

The Hyper Suprime-Cam (HSC) collaboration includes the astronomical communities of Japan and Taiwan, and Princeton University. The HSC instrumentation and software were developed by the National Astronomical Observatory of Japan (NAOJ), the Kavli Institute for the Physics and Mathematics of the Universe (Kavli IPMU), the University of Tokyo, the High Energy Accelerator Research Organization (KEK), the Academia Sinica Institute for Astronomy and Astrophysics in Taiwan (ASIAA), and Princeton University. Funding was contributed by the FIRST program from Japanese Cabinet Office, the Ministry of Education, Culture, Sports, Science and Technology (MEXT), the Japan Society for the Promotion of Science (JSPS), Japan Science and Technology Agency (JST), the Toray Science Foundation, NAOJ, Kavli IPMU, KEK, ASIAA, and Princeton University. This paper makes use of software developed for the Large Synoptic Survey Telescope. We thank the LSST Project for making their code freely available. The Pan-STARRS1 (PS1) Surveys have been made possible through contributions of the Institute for Astronomy, the University of Hawaii, the Pan-STARRS Project Office, the Max-Planck Society and its participating institutes, the Max Planck Institute for Astronomy and the Max Planck Institute for Extraterrestrial Physics, The Johns Hopkins University, Durham University, the University of Edinburgh, Queen’s University Belfast, the Harvard-Smithsonian Center for Astrophysics, the Las Cumbres Observatory Global Telescope Network Incorporated, the National Central University of Taiwan, the Space Telescope Science Institute, the National Aeronautics and Space Administration under Grant No. NNX08AR22G issued through the Planetary Science Division of the NASA Science Mission Directorate, the National Science Foundation under Grant No. AST-1238877, the University of Maryland, and Eotvos Lorand University (ELTE).

REFERENCES

- Abazajian, K., Adelman-McCarthy, J. K., Agüeros, M. A., et al. 2004, *AJ*, 128, 502
- Abbott, T., Abdalla, F. B., Allam, S., et al. 2016, *MNRAS*, in press (arXiv:1601.00329)
- Bechtol, K., Drlica-Wagner, A., Balbinot, E., et al. *ApJ*, 807, 50
- Belokurov, V., Zucker, D. B., Evans, N. W., et al. 2006, *ApJ*, 647, L11
- Bressan, A., Marigo, P., Girardi, L., et al. 2012, *MNRAS*, 427, 127
- Chabrier, G., 2001, *ApJ*, 554, 1274
- Drlica-Wagner, A., Bechtol, K., Rykoff, E. S., et al. 2015, *ApJ*, 813, 109
- Gilmore, G., Wilkinson, M. I., Wyse, R. F. G., et al. 2007, *ApJ*, 663, 948
- Gunn, J. E., & Stryker, L. L., 1983, *ApJS*, 52, 121
- Harris, W. E. 1996, *AJ*, 112, 1487
- Ivezic, Z., Axelrod, T., Brandt, W. N., et al. 2008, *AJ*, 176, 1
- Jordi, K., Grebel, E. K., Ammon, K. 2006, *ã*, 460, 339
- Juric, M., Ivezic, Z., Brooks, A., et al. 2008, *ApJ*, 673, 864
- Juric, M., Kantor, J., Lim, K.-T., et al. 2015, *ArXiv e-prints*, arXiv:1512.07914
- Kim, D., Jerjen, H., Milone, A. P. et al. 2015, *ApJ*, 803, 63
- Kim, D., & Jerjen, H. 2015, *ApJ*, 808, L39
- Klypin, A., Kravtsov, A. V., Valenzuela, O., & Prada, F. 1999, *ApJ*, 522, 82
- Koposov, S., Belokurov, V., Evans, N. W., et al. 2008, *ApJ*, 686, 279
- Koposov, S. E., Belokurov, V., Torrealba, G., & Evans, N. W. 2015, *ApJ*, 805, 130
- Kroupa, P., 2002, *Science*, 295, 82
- Laevens, B. P. M., Martin, N. F., Sesar, B., et al. 2014, *ApJ*, 786, L3
- Laevens, B. P. M., Martin, N. F., Ibata, R. A. et al. 2015a, *ApJ*, 802, L18
- Laevens, B. P. M., Martin, N. F., Bernard, E. J. et al. 2015b, *ApJ*, 813, L44
- Leauthaud, A., Massey, R., Kneib, J.-P., et al. 2007, *ApJS*, 172, 219
- Macciò, A. V., & Fontanot, F. 2010, *MNRAS*, 404, L16
- Magnier, E. A., Schlafly, E., Finkbeiner, D., et al. 2013, *ApJS*, 205, 20
- Martin, N. F., de Jong, J. T. A., & Rix, H.-W. 2008, *ApJ*, 684, 1075
- McConnachie, A. W., 2012, *AJ*, 144, 4
- Miyazaki, S., Komiyama, Y., Nakata, H., et al. 2012, *Proc. SPIE*, 8446, 84460Z
- Moore, B., Ghigna, S., Governato, F., Lake, G., Quinn, T., & Stadel, J. 1999, *ApJ*, 524, L19
- Sakamoto, T., & Hasegawa, T. 2006, *ApJ*, 653, L29
- Salpeter, E. E. 1955, *ApJ*, 121, 161
- Sawala, T., Frenk, C. S., & Fattahi, A., et al. 2016, *MNRAS*, 457, 1931
- Schlafly, E. F., & Finkbeiner, D. P. 2011, *ApJ*, 737, 103
- Schlafly, E. F., Finkbeiner, D. P., Jurić, M., et al. 2012, *ApJ*, 756, 158
- Schlegel, D. J., Finkbeiner, D. P., & Davis, M. 1998, *ApJ*, 500, 525
- Simon, J. D., & Geha, M. 2007, *ApJ*, 670, 313
- Tollerud, E. J., Bullock, J. S., Strigari, L. E., & Willman, B. 2008, *ApJ*, 688, 277
- Tonry, J. L., Stubbs, C. W., Lykke, K. R., et al. 2012, *ApJ*, 750, 99
- Walsh, S. M., Willman, B., & Jerjen, H. 2009, *AJ*, 137, 45
- Willman, B., Blanton, M. R., West, A. A., et al. 2005, *AJ*, 129, 2692
- York, D. G., Adelman, J., Anderson, J. E., Jr., et al. 2000, *AJ*, 120, 1579